# energy&fuels

# Tracking Changes in Asphaltene Nanoaggregate Size Distributions as a Function of Silver Complexation via Gel Permeation Chromatography Inductively Coupled Plasma Mass Spectrometry

Fang Zheng, Remi Moulian, Martha L. Chacón-Patiño, Ryan P. Rodgers, Caroline Barrère-Mangote, Murray R. Gray, Pierre Giusti, Quan Shi, and Brice Bouyssiere*

Read Online

ACCESS | Metrics & More | Article Recommendations | SI Supporting Information

**ABSTRACT:** Asphaltene elution behavior in gel permeation chromatography (GPC) was studied with and without the presence of silver triflate (AgOTf) via inductively coupled plasma mass spectrometry. The experiments highlighted the influence of AgOTf on the molecular weight profiles for atmospheric residues (ARs), asphaltenes, and their extrography subfractions. Specifically, the molecular weight distribution of the sulfur-, vanadium-, and nickel-containing compounds changed markedly with the addition of AgOTf, which suggests that AgOTf disrupts/alters the interaction between Ni and vanadyl porphyrins and select S-containing compounds within asphaltene nanoaggregates. However, similar effects were not observed with AgOTf addition to the high-molecular-weight GPC fractions of AR and the acetone extrography asphaltene fraction, which is comprised of abundant, highly aromatic/single-core compounds.
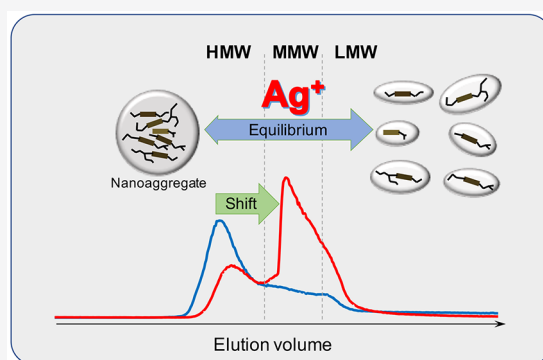


## INTRODUCTION

The molecular composition, structure, chemical functionalities, and properties of asphaltenes remain the most important issues in petroleum chemistry.[1−3] However, molecular characterization is hampered by aggregation, even in "favorable" solvents, which limits molecular characterization to those species that exist as free molecules in solution.[4] Previous studies of the unaggregated fraction of asphaltenes have revealed that the molecular weight of these molecules is not as high as previously suggested and is primarily distributed in the range of 500−1250 Da.[5] Past studies were now known to suffer from limitations imposed by the presence of aggregates, because the apparent molecular weight ranged from tens of thousands or even hundreds of thousands of daltons and changed with solvent composition.[6,7] Thus, future advances in molecular characterization will be enabled by methods that disrupt asphaltene aggregates and increase the analytical accessibility to the now free molecules that comprise them.

Morphological studies of asphaltene aggregates have received considerable attention from petroleum chemists for many years.[8,9] Various molecular-level structural models for asphaltene aggregates have been proposed,[9,10] despite their noted inconsistency with several asphaltene properties.[11] Regardless, the modified Yen model has emerged as one of the most cited/acknowledged representations of petroleum aggregates.[10,12] In this model, the primary interaction that drives aggregation is suggested to be the attraction between the large aromatic cores. This primary (interior) attractive force is

offset by the (exterior) repulsive forces that are attributed to the steric hindrance of peripheral alkyl side chains, which leads to a low number of molecules that make up the primary nanoaggregates (∼4−12 molecules). These nanoaggregates can subsequently form asphaltene clusters. Conversely, the model of asphaltene aggregates proposed by Gray et al.[11] suggests that asphaltenes undergo supramolecular assembly. In this model, asphaltene molecules produce multiple cooperative associations that are the sum of acid−base interactions, hydrogen bonding, metal coordination, hydrophobic pockets, and aromatic π−π stacks. Recently, Zhang et al.[13] proposed a pancake bonding model for the interpretation of asphaltene aggregation behavior based on the increased concentration of organic free radicals in asphaltenes relative to maltenes, which is consistent with the latest findings based on Fourier transform ion cyclotron resonance mass spectrometry (FT-ICR MS) and structural insights into asphaltene aromatic cores uniquely provided by non-contact atomic force microscopy techniques.[14−16] Despite decades of research, the architecture and molecular interactions responsible for asphaltene aggrega-
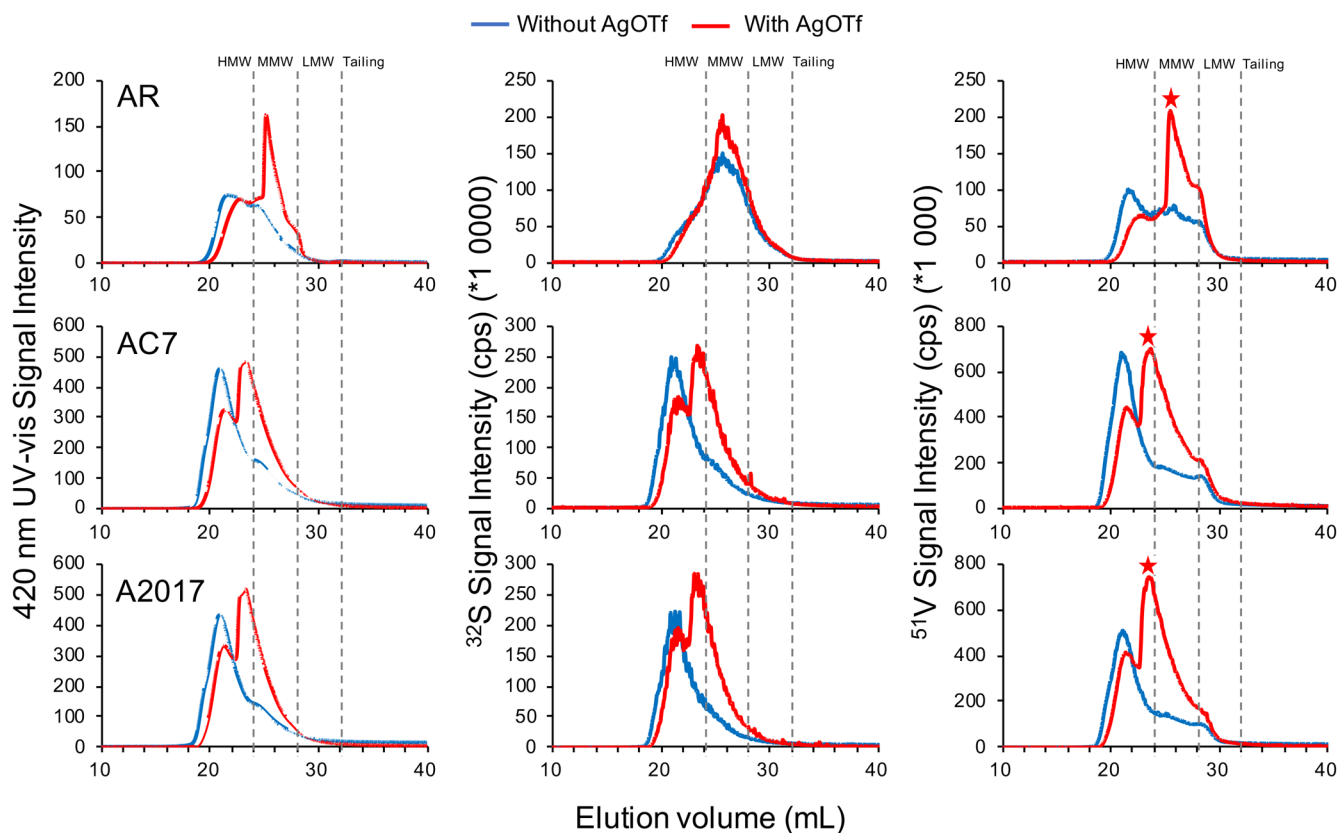
**Figure 1.** UV−vis absorption at 420 nm (left) and $^{32}$S (middle) and $^{51}$V (right) GPC−ICP−HRMS chromatograms of AR, AC7, and A2017 with (red trace) and without (blue trace) the addition of AgOTf. Gray dashed lines define the HMW, MMW, LMW, and tailing regions of the chromatogram. Red stars highlight differences in the $^{51}$V apex in the AR sample compared to the AC7 and A2017 asphaltene samples.

tion remain unresolved. However, the impact of asphaltene aggregation on the molecular understanding of these molecules is much clearer. It remains as one of the most significant impediments to understanding the structure and chemical functionally of those asphaltene molecules that contribute to aggregate formation.

Heteroatoms (primarily N, S, O, and metals, such as Ni and V) in petroleum have negative effects on downstream processes, especially in catalyst deactivation.[17−19] Hydro-demetalization (HDM) and hydrodesulfurization (HDS) processes can effectively remove metals and S elements from petroleum. However, in many cases, such heteroatoms are difficult to remove even under extremely harsh catalytic reaction conditions [>375 °C and $H_2$/oil (mL/L) > 500] and are attributed to those with extensive steric hindrance and/or those residing in asphaltene nanoaggregates.[20] Coupling gel permeation chromatography (GPC) with inductively coupled plasma high-resolution mass spectrometry (ICP−HRMS) provides unique insight into asphaltene nanoaggregate size distributions and quantitative information on heteroatom-containing species within.[21,22] The GPC aggregate size distribution, as determined by heteroatom detection via inductively coupled plasma mass spectrometry (ICP−MS), can be divided into high, medium, and low + tailing molecular weight fractions (HMW, MMW, and LMW, respectively), and quantitative studies for specific elements (commonly Ni, V, and S) are routinely performed to understand heteroatom composition as a function of the nanoaggregate size distribution.

Given the molecular characterization challenges imposed by aggregation, this work aims to shed light on the effect of silver cations on the aggregation state (monitored by changes of the elution behavior in GPC and detected for targeted elements by ICP−MS detection) for atmospheric residues, asphaltenes, and asphaltene extrography fractions. The focus on the influence of $Ag^+$ on the asphaltene aggregation state is guided by numerous studies that have documented the interactions of $Ag^+$ ions with aromatics, double bonds, or arenes,[23−25] polycyclic aromatic hydrocarbons (PAHs),[26,27] monoaromatics,[28] sulfur-containing compounds,[29,30] and saturates,[31] and porphyrins[32] The results suggest that $Ag^+$ can disrupt interactions that cause a shift in the distribution of nanoaggregates (originally present in the HMW region) toward lower apparent molecular weights that results in increased levels of "free" asphaltene molecules (in the MMW and LMW regions).

## ■ EXPERIMENTAL SECTION

**Reagents, Samples, and Materials.** *n*-Heptane ($C_7$) was used for asphaltene precipitation. Tetrahydrofuran (THF), toluene (Tol), and methanol (MeOH), all high-performance liquid chromatography (HPLC)-grade from J.T. Baker (Phillipsburg, NJ, U.S.A.), were used for asphaltene extrography fractionation. Tetrahydrofuran [THF, Multisolvent GPC grade, ACS, stabilized with 205 ppm of 2,6-di-*tert*-butyl-4-methylphenol (BHT), J.T. Baker, Phillipsburg, NJ, U.S.A.], was used for sample dilution prior to and as the mobile phase for GPC. Silver complexation was performed using silver triflate (AgOTf, Sigma-Aldrich).

**Asphaltene Sample Preparation.** Asphaltene samples (AC7 and A2017) were isolated from the Middle East crude oil by ASTM D6560-12. Once dried under $N_2$ (g), the Petrophase 2017 (A2017)

asphaltenes[33] was subsequently crushed and exhaustively washed with hot heptane (200 mL, Soxhlet extraction) in 5 h intervals until the extraction yielded <0.2 mg/200 mL heptane. After each extraction cycle, the remnant asphaltenes were crushed and fresh heptane was added to aide in the further removal of entrained/co-precipitated maltenes. Atmospheric residue was the AR obtain from the same Middle East oil. Elemental analysis of the atmospheric residue and its asphaltene fraction has been previously described and is included in Table S1 of the Supporting Information.[34]

**Asphaltene Fractionation by Extrography.** The asphaltene sample A2017 was adsorbed on silica gel at a mass loading of 1%. The dried mixture was then extracted in a Soxhlet apparatus using a series of three different solvents: acetone (100%), Hep/Tol (1:1), and Tol/THF/MeOH (10:10:1). An extended version of the extrography method is reported elsewhere.[35] These three fractions, which were named ACE, C$_7$T, and TTM, were dried under nitrogen and stored in the dark for subsequent analyses.[34]

**Preparatory GPC Fractionation for the AR and Asphaltenes.** GPC fractionation was performed with an AKTA purifier liquid chromatography system equipped with a UV-900 multiwavelength ultraviolet (UV) absorbance detector and a Frac-950 fraction collector (GE Healthcare Bio-Sciences, Pittsburgh, PA, U.S.A.). Three polymeric Shodex preparative GPC columns were connected in series. The mobile phase consisted of 100% ACS xylene. Preparative-scale separations were performed at a flow rate of 3 mL/min.[36]

**HDS and HDM Processes.** A hydrotreatment study was performed at the pilot scale on the AR sample. Two reactor pilots were used, which allowed for the sampling of intermediate effluent after the first reactor (Eff 1) and total effluent (Eff 2). On the basis of the prior experience with the hydrotreatment of AR in fixed bed units, the reactors were loaded with a large pore hydrodemetalation catalyst in the first reactor and a smaller pore transition reactor and hydrodesulfurization catalyst in the second reactor.

**Silver Triflate Addition.** The AR and asphaltene samples and their extrography samples were diluted in THF to a concentration of 20 mg/g. The preparative GPC subfractions of AR and asphaltenes were diluted in THF to a concentration of 5 mg/g. AgOTf (Sigma-Aldrich) experiments were performed at a final concentration of 100 ppm.[32]

**GPC-ICP-MS/UV Analysis.** The chromatographic system was composed of a Dionex HPLC system with an UltiMate 3000 microflow pump, an UltiMate 3000 autosampler, a low port-to-port dead-volume microinjection valve, and an Ultimate UV system (at the 420 nm wavelength). Three GPC columns (from 1000 to 600 000 Da) connected in series were used. A Styragel guard column (4.6 mm inner diameter, 30 mm length, and 10 000 Da exclusion limit) was applied before the columns, and the flow rate was 1 mL min$^{-1}$ for 90 min. A splitter of 1/20 was used to send only 40 $\mu$L min$^{-1}$ into a double-focusing sector field inductively coupled high-resolution plasma mass spectrometer (ICP-HRMS, Element XR, Thermo Fisher Scientific, Germany). The samples were analyzed as solutions prepared 2 days before injection to ensure that the reaction with silver proceeded. The detailed instrument parameters and operating procedures have been previously described.[32]

## RESULTS AND DISCUSSION

**Ag+ Addition to the AR and Asphaltenes.** Figure 1 shows the GPC-ICP-MS [center ($^{32}$S) and right ($^{51}$V)] and ultraviolet–visible (UV–vis) absorption (left, at 420 nm) chromatograms for the AR (top), AC7 (middle), and A2017 (bottom row) with (red trace) and without (blue trace) the addition of AgOTf. As a reminder, AC7 and A2017 are asphaltenes derived from the same AR, but A2017 underwent additional washing steps. The unspiked AR sample (top row, blue trace) contains abundant HMW aggregates as detected by both the $^{51}$V ICP-MS and UV-vis detection that indicates the presence large nanoaggregates. Table 1 includes integration

**Table 1. Molecular Weight Distribution of $^{32}$S and $^{51}$V in the Chromatograms of AR, AC7, and A2017**

| | sample | | HMW area (%) | MMW area (%) | LMW area (%) | tailing area (%) |
|---|---|---|---|---|---|---|
| S | AR | no AgOTf | 26.4 | 57.0 | 12.8 | 3.8 |
| | | AgOTf | 20.6 | 63.3 | 13.4 | 2.8 |
| | AC7 | no AgOTf | 69.5 | 16.9 | 4.3 | 9.4 |
| | | AgOTf | 59.7 | 31.6 | 5.2 | 3.4 |
| | A2017 | no AgOTf | 69.5 | 14.5 | 3.8 | 12.2 |
| | | AgOTf | 63.7 | 28.8 | 3.9 | 3.6 |
| V | AR | no AgOTf | 46.8 | 38.6 | 8.3 | 6.3 |
| | | AgOTf | 24.4 | 65.7 | 8.8 | 1.1 |
| | AC7 | no AgOTf | 63.0 | 19.6 | 6.3 | 11.2 |
| | | AgOTf | 53.0 | 36.4 | 7.0 | 3.5 |
| | A2017 | no AgOTf | 60.8 | 18.6 | 6.1 | 14.6 |
| | | AgOTf | 55.8 | 34.6 | 5.7 | 3.8 |

areas (IAs) for all of the analyses and facilitates quantitative sample comparisons. However, S-containing compounds are most abundant (57% IA) in MMW aggregates, with the remainder split between the HMW (26.4% IA) and LMW + tailing (16.6% IA) regions; thus, S is most abundant in the MMW aggregates, whereas Ni and V are most abundant in the HMW region (larger aggregates). The elution profile of the unspiked asphaltenes was shifted toward the HMW region and displayed a maximum for UV−vis absorption, $^{32}$S, and $^{51}$V. The asphaltene profiles for the S species (maximum in HMW) differ from that of the AR (maximum in MMW) and are more similar to the asphaltene $^{51}$V and UV−vis chromatograms (maximum in HMW), which suggests that AR is composed of abundant S-containing species with low/weak aggregation tendencies (attributed to maltenes). Simply, isolation of the asphaltenes from the AR yields S-containing compounds that primarily exist as large nanoaggregates, which elute in the HMW region.

After the addition of AgOTf (red traces in Figure 1 and Figure S1 of the Supporting Information for Ni), the V species shifted significantly from the HMW fraction to the MMW fraction in the AR (from 38.6 to 65.7% IA) and asphaltenes (from ~21 to 35.5% IA). The shift of S species in AR was far less obvious because the main proportion of S-containing compounds already resides in the MMW region; the loss of 5.8% IA in the HMW region yielded a commensurate (albeit slight) increase of 6.3% IA in the MMW region. Changes in the LMW and tailing regions were at or below 1% IA. Thus, the S species were mostly distributed in the MMW area, with few HMW asphaltene nanoaggregates. The GPC−ICP−MS and UV−vis absorption chromatograms of $^{58}$Ni and $^{109}$Ag for AR, AC7, and A2017 with and without the addition of AgOTf are shown in Figure S1 of the Supporting Information. The retention time of the peaks that appeared after silver addition in both $^{51}$V (right column in Figure 1) and $^{58}$Ni (left column in Figure S1 of the Supporting Information) in the asphaltene samples (where disruption of larger aggregates was observed) is different from that of the AR sample (where little disruption occurred), which suggests that the disaggregation process was promoted by silver cations. Additional evidence is provided by the $^{109}$Ag chromatograms (right column in Figure S1 of the Supporting Information) that reveal that the majority of the spiked Ag cations elute with the HMW aggregates for the asphaltene samples, whereas in the AR, they reside in the MMW region. Interestingly, although Ag cations clearly bind
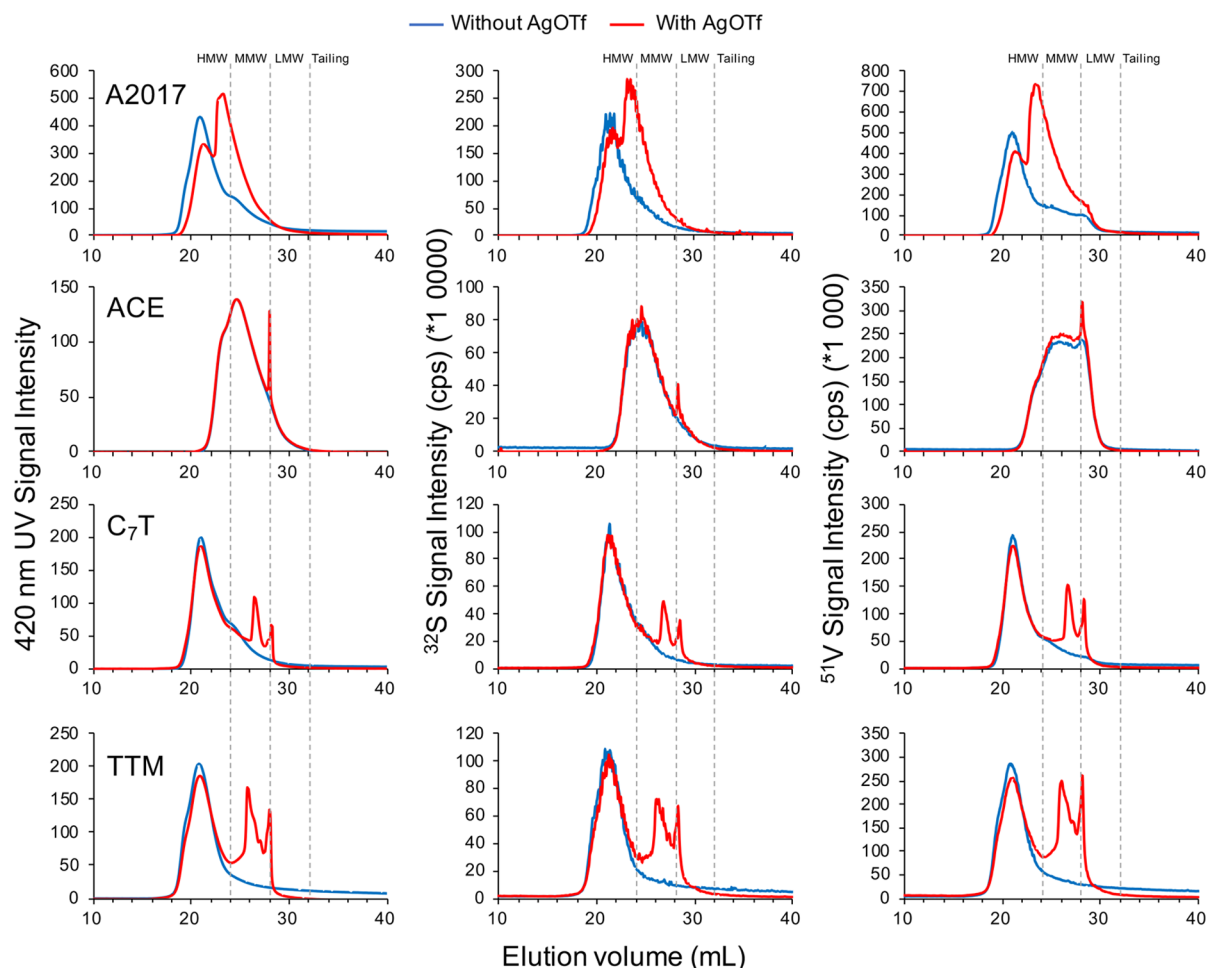
**Figure 2.** UV−vis absorption at 420 nm (left) and $^{32}$S (middle) and $^{51}$V (right) GPC−ICP−HRMS chromatograms of A2017, ACE, C$_7$T, and TTM with (red trace) and without (blue trace) the addition of AgOTf.

**Table 2. Molecular Weight Distribution of $^{32}$S and $^{51}$V in the Chromatograms of A2017, ACE, C$_7$T, and TTM**

|   | sample |  | HMW area (%) | MMW area (%) | LMW area (%) | tailing area (%) |
|---|--------|--------|------|------|------|------|
| S | A2017 | no AgOTf | 69.5 | 14.5 | 3.8 | 12.2 |
|   |       | AgOTf | 63.7 | 28.8 | 3.9 | 3.6 |
|   | ACE | no AgOTf | 37.7 | 55.7 | 6.6 | 0.1 |
|   |     | AgOTf | 35.7 | 53.2 | 9.2 | 1.9 |
|   | C$_7$T | no AgOTf | 73.1 | 15.6 | 3.6 | 7.7 |
|   |      | AgOTf | 68.2 | 24.7 | 5.4 | 1.6 |
|   | TTM | no AgOTf | 71.2 | 9.3 | 5.2 | 14.3 |
|   |     | AgOTf | 61.6 | 33.1 | 5.1 | 0.1 |
| V | A2017 | no AgOTf | 60.8 | 18.6 | 6.1 | 14.6 |
|   |       | AgOTf | 55.8 | 34.6 | 5.7 | 3.8 |
|   | ACE | no AgOTf | 18.7 | 65.3 | 16.0 | 0.0 |
|   |     | AgOTf | 18.4 | 64.4 | 16.5 | 0.6 |
|   | C$_7$T | no AgOTf | 69.1 | 15.2 | 4.8 | 10.9 |
|   |      | AgOTf | 62.8 | 30.1 | 5.9 | 1.2 |
|   | TTM | no AgOTf | 67.4 | 10.3 | 5.8 | 16.5 |
|   |     | AgOTf | 55.5 | 39.8 | 4.7 | 0.0 |

to AR HMW aggregates (top right panel in Figure S1 of the Supporting Information), they appear to selectively liberate Ni- and V-containing species, with the S-containing compounds nearly unchanged. Precipitation of asphaltenes from the AR to obtain AC7 selectively isolates V, Ni, and S HMW compounds

in the asphaltenes, and thus, the GPC elution profile shifts toward HMW. A further comparison between AC7 and A2017 elution behavior suggests that the presence of occluded/co-precipitated maltenes does not dramatically affect the asphaltene elution profiles, because A2017 was subjected to exhaustive Soxhlet extraction with heptane to decrease the amount of co-precipitated maltenic material. Thus, apparently the "washing" step does not drastically affect the GPC results. Before and after Ag addition, the profiles of AC7 and A2017 are remarkably similar. This is in stark contrast to molecular characterization experiments performed by high-resolution mass spectrometry, most frequently FT-ICR MS, where the presence of low levels of co-precipitated maltenes can mask the detection of the much more abundant asphaltenes as a result of selective ionization.[37] Finally, the apex for the $^{51}$V peaks for the three samples (AR, AC7, and A2017) spiked with Ag$^+$ (red traces in the right column in Figure 1) are located at two different elution volumes (∼25.5 mL for AR and 23.5 mL for both AC7 and A2017 asphaltenes) highlighted with red stars. A similar behavior is noted for $^{58}$Ni in the left column in Figure S1 of the Supporting Information. The addition of Ag$^+$ to AR leads to species with a higher retention volume (25.5 mL, lower apparent molecular weight) than the two asphaltene samples (23.5 mL, higher apparent molecular weight), which suggests that disruption of the AR aggregates yields smaller aggregates compared to the asphaltenes. Of note, these
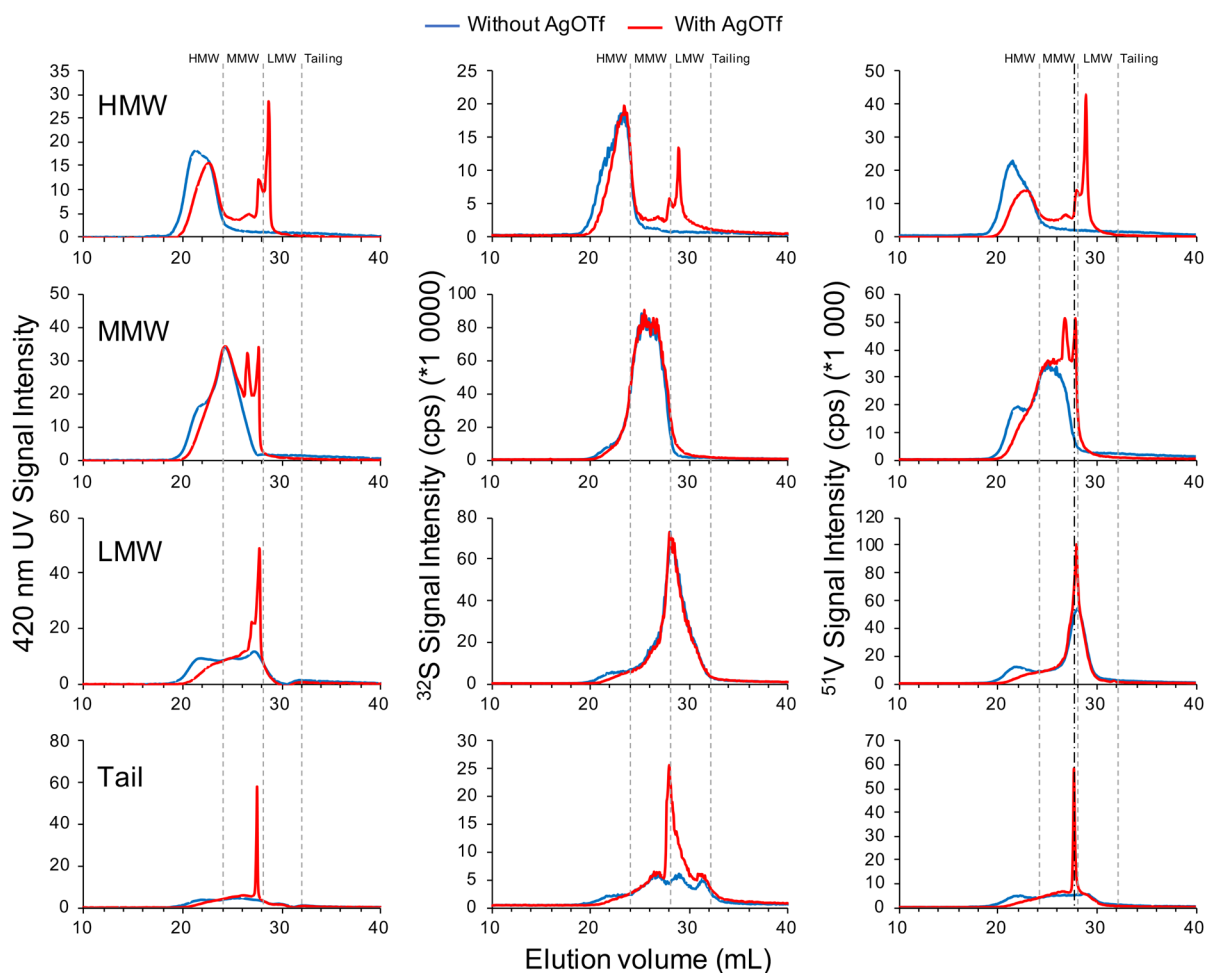
**Figure 3.** UV−vis absorption at 420 nm and $^{32}S$ and $^{51}V$ GPC−ICP−HRMS chromatograms of preparative GPC fractions of AR with and without the addition of AgOTf.

products are still termed aggregates, because a nearly identical analysis performed by online GPC FT-ICR MS detected "free" porphyrin molecules at elution volumes of >27 mL.[38] Although the addition of $Ag^+$ clearly shifts the $^{51}V$ elution profile toward lower apparent molecular weights for the asphaltene samples, the apex of both still resides in the HMW region. Consequently, the products of the aggregate disruption remain aggregated to some extent.

In summary, the data shown in Table 1 suggest a decrease in the amount of HMW compounds and an increase in the percentage of MMW and LMW compounds upon $Ag^+$ addition. It is worth noting that the tailing area was larger than the LMW area for AC7 and A2017 without AgOTf, which may be related to the interaction between certain petroleum molecules and the GPC column. The percentage of the tailing region decreased with the addition of $Ag^+$ ions, which indicated that $Ag^+$ ions may help to eliminate this interaction.

**$Ag^+$ Addition to Asphaltene Extrography Fractions.** Extraction of the acetone-soluble fraction of A2017 asphaltenes adsorbed on $SiO_2$ (extrography fraction ACE) has previously been shown to yield a highly aromatic fraction dominated by island-type molecules, with readily detectable metalloporphyrins and sulfur-containing molecules in the MMW and LMW + tailing GPC regions by mass spectrometry.[34,39] Such behavior is confirmed by the GPC−ICP−MS results presented in the far right, second from top panel in Figure 2 that shows that the

acetone extrography fraction uniquely elutes in the MMW and LMW regions (free molecule regions), where AgOTf addition has little influence on the S and $^{51}V$ traces (shown in red). Similar behavior is also noted for $^{58}Ni$ in Figure S2 of the Supporting Information, where no shift in the molecular weight distribution occurred in the ACE fraction when AgOTf was added, except for a similar peak appearing in the LMW region (~28 mL elution volume). Thus, as also seen in Table 2, the ACE extrography fraction has a low degree of aggregation with a high mass fraction of "free" molecules for which AgOTf has little effect on the molecular weight distribution, except for liberation of S, V, and Ni species at 28 mL elution volume.

Conversely, the majority of S, V, and Ni compounds in the $C_7T$ and TTM extrography fractions elute in the HMW GPC region (Figure 2 and Figure S2 of the Supporting Information and Table 2) and demonstrate the greatest changes upon AgOTf addition. Specifically, S, V, and Ni display a shift to the MMW and LMW regions after AgOTf was added, despite having a prominent base peak that remains in the HMW region. However, a considerable amount of these aggregates was difficult to disassociate by $Ag^+$ ions. The GPC−ICP−MS and UV chromatograms of Ni and Ag of A2017, ACE, $C_7T$ and TTM with and without the addition of AgOTf are shown in Figure S2 of the Supporting Information. The addition of AgOTf shows that some S and V species can be released from
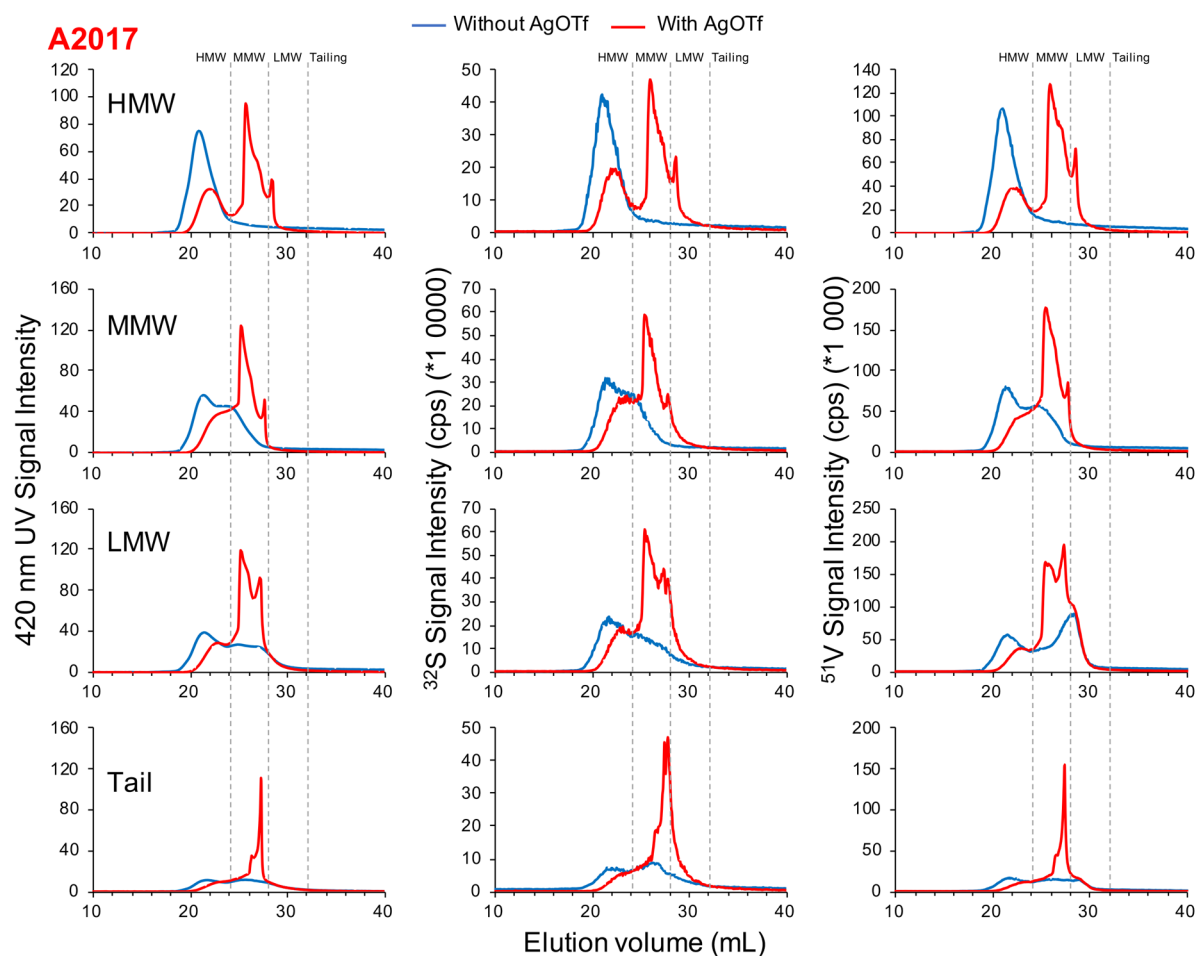
**Figure 4.** UV−vis absorption at 420 nm and $^{32}$S and $^{51}$V GPC−ICP−HRMS chromatograms of preparative GPC fractions of A2017 with and without the addition of AgOTf.

**Table 3. Molecular Weight Distribution of $^{51}$V in the Reinjection Chromatograms for the LMW Subfractions of AR, AC7, and A2017**

| | sample | HMW area (%) | MMW area (%) | LMW area (%) | tailing area (%) |
|---|---|---|---|---|---|
| AR | no AgOTf | 21.3 | 46.6 | 23.3 | 8.8 |
| | AgOTf | 10.5 | 63.8 | 21.8 | 3.8 |
| AC7 | no AgOTf | 26.8 | 40.8 | 22.9 | 9.4 |
| | AgOTf | 11.3 | 66.2 | 20.8 | 1.8 |
| A2017 | no AgOTf | 33.1 | 36.1 | 17.1 | 13.7 |
| | AgOTf | 13.7 | 70.5 | 13.9 | 2.0 |

the nanoaggregates. This result is in agreement with the presence of this species linked/associated with the surface of the nanoaggregate.[34] In the C$_7$T and TTM fractions, most V porphyrins seem to be trapped in the aggregates and not accessible to AgOTf. This finding is consistent with the results obtained by Chacón-Patiño et al., where the poor ionization of this HMW region of the GPC chromatogram increased the difficulty of characterizing the V porphyrin compounds by (+) atmospheric pressure photoionization (APPI) FT-ICR MS, which is well-known to be hampered by nanoaggregation (Table 2).[38]

**Reinjection of Preparative-Scale GPC Subfractions.**
To further study the influence of Ag$^+$ ions on aggregate elution

profiles, the AR and asphaltene samples were separated into HMW, MMW, LMW, and tailing subfractions by preparative-scale GPC. Reinjection of the isolated HMW, MMW, and LMW fractions with and without Ag$^+$ addition provides insight into the contribution of each fraction to the changes documented in Figure 1 as well as any changes in the aggregation elution profiles (reaggregation or disaggregation) that might occur after isolation of the individual subfractions (HMW, MMW, LMW, and tailing).

For the AR sample subfractions, Figure 3 shows the UV−vis absorption at 420 nm and the S and V GPC−ICP−HRMS chromatograms for the reinjected HMW, MMW, LMW, and tailing fractions initially isolated by preparative-scale GPC of the AR sample. Figure S4 of the Supporting Information and Figure 4 show similar chromatograms but for the AC7 and A2017 asphaltene subfractions, respectively. As previously reported,[21,36] the reinjection of the HMW, MMW, LMW, and tailing fractions show that the HMW fraction elutes again in the HMW region and, thus, shows the stability of these nanoaggregates after evaporation and dilution for reinjection. The MMW fraction partially elutes with the HMW region, thus showing a possible reaggregation of part of this fraction. LMW is also mainly in the HMW/MMW region of the chromatogram but with some reaggregation that was more present in asphaltene than in AR samples, which could be clearly seen by the molecular weight distribution of the LMW subfraction
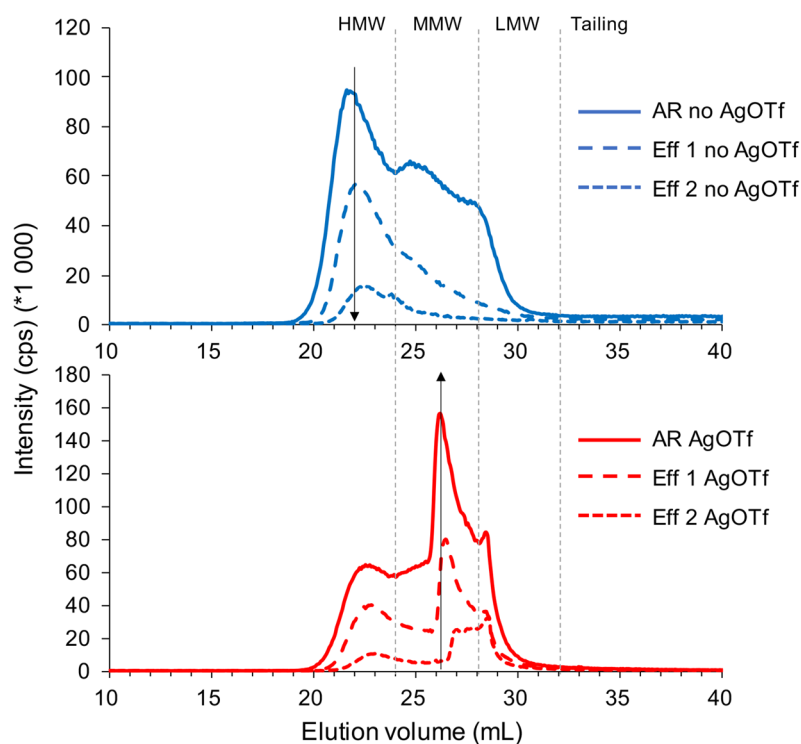
**Figure 5.** Graphs of AR, Eff 1, and Eff 2 with and without AgOTf for V (Ar, solid line; Eff 1, dashed line; and Eff 2, dotted line).

**Table 4. Total Area of Sulfur and Vanadium Chromatograms for AR to Eff 1 and Eff 2 and Decrease in the Area from AR to Eff 1 and Eff 2**

|   | sample | AR | Eff 1 | Eff 2 |
|---|---|---|---|---|
| S | total area | 12924640 | 7027570 | 2225840 |
|   | decrease (%) |  | 45.6 | 82.8 |
| V | total area | 622090 | 257000 | 70060 |
|   | decrease (%) |  | 58.7 | 88.7 |

reinjection in Table 3. The GPC−ICP mass chromatograms of the reinjected HMW, MMW, LMW, and tailing fractions of AR, AC7, and A2017 are shown in Figures S7, S8, S9, and S10 of the Supporting Information, respectively. The tailing fraction elutes after the permeation volume of the GPC column; therefore, this fraction corresponds to compounds or nanoaggregates that interact with the phase of the GPC column. After evaporation and reinjection of this fraction, the main compounds are now eluting in the HMW, MMW, and LMW regions of the chromatogram, thus showing that these compounds can form nanoaggregates that have less interaction with the column and, thus, elute earlier in the chromatogram. The addition of Ag to this fraction leads to a small disaggregation that produces an intense peak at 28 min (tailing profiles in Figure 3).

The effect of Ag$^+$ ions was less prominent for the GPC subfractions (HMW, MMW, LMW, and tailing) of AR than for these subfractions in the asphaltene samples. The main effect appears to occur in the HMW fraction, with disappearance of the earliest eluting species and subsequent increase in the LMW region. This finding clearly shows disaggregation, which is assumed to be molecules on the periphery of the nanoaggregates, as previously reported by Moulian et al.[32] The MMW and LMW fractions present very little difference in the S chromatogram between AgOTf addition and no AgOTf

addition, thus showing that these fractions are stable under the conditions used. Concerning the UV and $^{51}$V traces for the HMW component of the reinjected LMW and MMW fractions, both fractions exhibit disaggregation of a fraction of the HMW aggregates to yield increases in the LMW region. Thus, the results suggest that a part of this HMW fraction is associated with a weaker reaggregation process and not with the formation of stable nanoaggregates in solution. Finally, for the tailing fraction, the effect of Ag$^+$ ions also leads to a small amount of disaggregation of the HMW part to the LMW part.

However, the modifications induced by Ag$^+$ ions on the GPC subfractions of AC7 and A2017 were much more pronounced, as shown in Figure 4 and Figures S4−S6 of the Supporting Information. Each profile of these subfractions showed a significant shift from HMW to MMW and/or LMW, which indicated that, although the Ag$^+$ ion poorly modifies the original nanoaggregates in AR, it can disrupt a larger fraction of nanoaggregates formed during asphaltene precipitation.

**Effect of Ag$^+$ Addition to Hydrotreated Materials.** Sulfur and metal elements in AR can be effectively removed by hydrotreatment. As shown in Figure 5 and Figure S11 of the Supporting Information, the abundance of S and V species decreased in Eff 1 and was much lower in Eff 2, with a more severe reaction. The specific area and decrease in the area from AR to Eff 1 and Eff 2 are shown in Table 4. However, no change in the molecular weight distribution of S species was observed before and after hydrotreatment, and they were mainly distributed in the MMW region. Moreover, for sulfur, no obvious change occurred in the GPC elution profiles with the addition of AgOTf.

Concerning the UV and V chromatograms, species in the MMW and LMW regions were the first removed in the hydrotreatment, as previously reported.[20,40] In Eff 1 and Eff 2, most V species eluted in the HMW region. Although the proportion of V species in the MMW and LMW regions

increased with the addition of AgOTf, the fraction of V species in the HMW region remains. Thus, Ag$^+$ ions cannot fully disaggregate asphaltene nanoaggregates even after extensive hydrotreatment. However, the unique shifts in the profiles for V in the hydrotreated samples (Eff 1 and Eff 2) indicated that, as the HMW is consumed, there is a concurrent effect on the amount of $^{51}$V species that reports to the MMW and LMW regions. Simply, with more extensive hydrotreatment, the level of disaggregated material that elute in the MMW region induced by Ag$^+$ addition is markedly decreased and the fraction that elutes in the LMW region is relatively unchanged.

## CONCLUSION

The GPC−ICP−MS analysis of an atmospheric residue with and without the addition of Ag$^+$ tested the ability of Ag$^+$ to disrupt "native" aggregates that exist in the whole AR sample (prior to asphaltene precipitation and fractionation). The results suggest that Ag$^+$ has very little effect on sulfur-containing species but disrupts some part of the HMW material to liberate V and Ni species that then elute primarily in the MMW region as well as a small fraction in the LMW region. Such differences in the metal-containing species relative to the sulfur-containing species suggest that a larger mass fraction of the metal-containing species is either exclusively held in less stable nanoaggregates or that they are weakly bound to the surface-accessible regions of the nanoaggregates. However, analysis of two different asphaltenes (with differing levels of washing) isolated from the AR revealed similar changes to both sulfur- and metal-containing species with Ag$^+$ addition. Thus, isolation of the asphaltene fraction from the AR yielded different results from analysis of the whole AR. Subsequent fractionation of the asphaltenes by an extrography method isolated the unique disruption of S-containing species with Ag$^+$ addition to the C$_7$T and TTM fractions, which display much higher levels of aggregation relative to the ACE fraction. Thus, the larger aggregates have some mass fraction of metal- and sulfur-containing species that can be liberated with Ag$^+$ addition. The ACE asphaltene fraction had a GPC elution profile most similar to the original AR and, thus, had similarly poor performance with Ag$^+$ addition, where very little differences were observed. Such trends were confirmed by reinjection experiments of preparatory-scale GPC separations; the HMW fractions showed the greatest effect with Ag$^+$ addition with both metal- and sulfur-containing species eluting in the LMW region and a concurrent loss of material in the HMW region. Finally, these same trends were shown in a series of hydrotreated AR samples at differing process severity. Simply, regardless of severity, Ag$^+$ addition had little to no effect on the sulfur-containing species, which were primarily in smaller nanoaggregates that eluted in the MMW range. Conversely, the metal-containing species, which eluted primarily in the HMW range (larger nanoaggregates), showed a marked effect of Ag$^+$ addition, with liberated species eluting in both the MMW and LMW regions. Collectively, the data suggests that the nanoaggregates that elute in the MMW region are least affected by Ag$^+$ addition. Larger aggregates (in the HMW region) are most affected by Ag$^+$ addition and yield both metal- and sulfur-containing species that elute in later (lower molecular weight) regions of the GPC chromatogram.

## ASSOCIATED CONTENT

### Supporting Information

The Supporting Information is available free of charge at https://pubs.acs.org/doi/10.1021/acs.energyfuels.1c02173.

AR bulk analysis and Ni and Ag GPC−ICP−MS chromatograms that are not present in the paper (PDF)

## AUTHOR INFORMATION

### Corresponding Author

**Brice Bouyssiere** − *Energy and Environment Solutions (E2S), Université de Pau et des Pays de l'Adour (UPPA), Centre National de la Recherche Scientifique (CNRS), Institut des Sciences Analytiques et de Physicochimie pour l'Environnement et les Matériaux (IPREM), UMR 5254, 64053 Pau, France; International Joint Laboratory C2MC: Complex Matrices Molecular Characterization, Total Research & Technology, F-76700 Harfleur, France;* orcid.org/0000-0001-5878-6067; Phone: +33-0-559-407-752; Email: brice.bouyssiere@univ-pau.fr

### Authors

**Fang Zheng** − *Energy and Environment Solutions (E2S), Université de Pau et des Pays de l'Adour (UPPA), Centre National de la Recherche Scientifique (CNRS), Institut des Sciences Analytiques et de Physicochimie pour l'Environnement et les Matériaux (IPREM), UMR 5254, 64053 Pau, France; State Key Laboratory of Heavy Oil Processing, China University of Petroleum, Beijing 102249, People's Republic of China; Petrochemical Research Institute of PetroChina Company, Limited, Beijing 102206, People's Republic of China*

**Remi Moulian** − *Energy and Environment Solutions (E2S), Université de Pau et des Pays de l'Adour (UPPA), Centre National de la Recherche Scientifique (CNRS), Institut des Sciences Analytiques et de Physicochimie pour l'Environnement et les Matériaux (IPREM), UMR 5254, 64053 Pau, France; International Joint Laboratory C2MC: Complex Matrices Molecular Characterization, Total Research & Technology, F-76700 Harfleur, France; Total Research & Technology, F-76700 Harfleur, France;* orcid.org/0000-0002-8042-7607

**Martha L. Chacón-Patiño** − *International Joint Laboratory C2MC: Complex Matrices Molecular Characterization, Total Research & Technology, F-76700 Harfleur, France; National High Magnetic Field Laboratory and Future Fuels Institute, Florida State University, Tallahassee, Florida 32310, United States;* orcid.org/0000-0002-7273-5343

**Ryan P. Rodgers** − *Energy and Environment Solutions (E2S), Université de Pau et des Pays de l'Adour (UPPA), Centre National de la Recherche Scientifique (CNRS), Institut des Sciences Analytiques et de Physicochimie pour l'Environnement et les Matériaux (IPREM), UMR 5254, 64053 Pau, France; International Joint Laboratory C2MC: Complex Matrices Molecular Characterization, Total Research & Technology, F-76700 Harfleur, France; National High Magnetic Field Laboratory and Future Fuels Institute, Florida State University, Tallahassee, Florida 32310, United States;* orcid.org/0000-0003-1302-2850

**Caroline Barrère-Mangote** − *International Joint Laboratory C2MC: Complex Matrices Molecular Characterization,*

*Total Research & Technology, F-76700 Harfleur, France;*
*Total Research & Technology, F-76700 Harfleur, France*

**Murray R. Gray** − *Department of Chemical and Materials Engineering, University of Alberta, Edmonton, Alberta T6G 1H9, Canada*

**Pierre Giusti** − *Energy and Environment Solutions (E2S), Université de Pau et des Pays de l'Adour (UPPA), Centre National de la Recherche Scientifique (CNRS), Institut des Sciences Analytiques et de Physicochimie pour l'Environnement et les Matériaux (IPREM), UMR 5254, 64053 Pau, France; International Joint Laboratory C2MC: Complex Matrices Molecular Characterization, Total Research & Technology, F-76700 Harfleur, France; Total Research & Technology, F-76700 Harfleur, France;*
   orcid.org/0000-0002-9569-3158

**Quan Shi** − *State Key Laboratory of Heavy Oil Processing, China University of Petroleum, Beijing 102249, People's Republic of China;*   orcid.org/0000-0002-1363-1237

Complete contact information is available at:
https://pubs.acs.org/10.1021/acs.energyfuels.1c02173

**Notes**

The authors declare no competing financial interest.

## ■ REFERENCES

(1) Chilingarian, G. V.; Yen, T. F. *Bitumens, Asphalts, and Tar Sands*; Elsevier: Amsterdam, Netherlands, 1978.

(2) Rogel, E.; Miao, T.; Vien, J.; Roye, M. Comparing asphaltenes: Deposit versus crude oil. *Fuel* **2015**, *147*, 155−160.

(3) Rogel, E.; Roye, M.; Vien, J.; Miao, T. Characterization of Asphaltene Fractions: Distribution, Chemical Characteristics, and Solubility Behavior. *Energy Fuels* **2015**, *29* (4), 2143−2152.

(4) Gray, M. R.; Yarranton, H. W.; Chacón-Patiño, M. L.; Rodgers, R. P.; Bouyssiere, B.; Giusti, P. Distributed Properties of Asphaltene Nanoaggregates in Crude Oils: A Review. *Energy Fuels* **2021**, DOI: 10.1021/acs.energyfuels.1c01837.

(5) Mullins, O. C.; Martínez-Haya, B.; Marshall, A. G. Contrasting Perspective on Asphaltene Molecular Weight. This Comment vs the Overview of A. A. Herod, K. D. Bartle, and R. Kandiyoti. *Energy Fuels* **2008**, *22* (3), 1765−1773.

(6) Badre, S.; Carla Goncalves, C.; Noringa, K.; Gustavson, G.; Mullins, O. C. Molecular size and weight of asphaltene and asphaltene solubility fractions from coals, crude oils and bitumen. *Fuel* **2006**, *85* (1), 1−11.

(7) Strausz, O. P.; Peng, P. a.; Murgich, J. About the Colloidal Nature of Asphaltenes and the MW of Covalent Monomeric Units. *Energy Fuels* **2002**, *16* (4), 809−822.

(8) *Asphaltene Deposition: Fundamentals, Prediction, Prevention, and Remediation*; Vargas, F. M., Tavakkoli, M., Eds.; CRC Press: Boca Raton, FL, 2018; DOI: 10.1201/9781315268866.

(9) Yen, T. F.; Erdman, J. G.; Pollack, S. S. Investigation of the Structure of Petroleum Asphaltenes by X-ray Diffraction. *Anal. Chem.* **1961**, *33* (11), 1587−1594.

(10) Mullins, O. C. The Modified Yen Model. *Energy Fuels* **2010**, *24* (4), 2179−2207.

(11) Gray, M. R.; Tykwinski, R. R.; Stryker, J. M.; Tan, X. Supramolecular Assembly Model for Aggregation of Petroleum Asphaltenes. *Energy Fuels* **2011**, *25* (7), 3125−3134.

(12) Rashid, Z.; Wilfred, C. D.; Gnanasundaram, N.; Arunagiri, A.; Murugesan, T. A comprehensive review on the recent advances on the petroleum asphaltene aggregation. *J. Pet. Sci. Eng.* **2019**, *176*, 249−268.

(13) Zhang, Y.; Siskin, M.; Gray, M. R.; Walters, C. C.; Rodgers, R. P. Mechanisms of Asphaltene Aggregation: Puzzles and a New Hypothesis. *Energy Fuels* **2020**, *34* (8), 9094−9107.

(14) Schuler, B.; Meyer, G.; Peña, D.; Mullins, O. C.; Gross, L. Unraveling the Molecular Structures of Asphaltenes by Atomic Force Microscopy. *J. Am. Chem. Soc.* **2015**, *137* (31), 9870−9876.

(15) Zhang, Y.; Schulz, F.; Rytting, B. M.; Walters, C. C.; Kaiser, K.; Metz, J. N.; Harper, M. R.; Merchant, S. S.; Mennito, A. S.; Qian, K.; Kushnerick, J. D.; Kilpatrick, P. K.; Gross, L. Elucidating the Geometric Substitution of Petroporphyrins by Spectroscopic Analysis and Atomic Force Microscopy Molecular Imaging. *Energy Fuels* **2019**, *33* (7), 6088−6097.

(16) Zhang, Y. Nonalternant Aromaticity and Partial Double Bond in Petroleum Molecules Revealed: Theoretical Understanding of Polycyclic Aromatic Hydrocarbons Obtained by Noncontact Atomic Force Microscopy. *Energy Fuels* **2019**, *33* (5), 3816−3820.

(17) Ok, S.; Mal, T. K. NMR Spectroscopy Analysis of Asphaltenes. *Energy Fuels* **2019**, *33* (11), 10391−10414.

(18) Nascimento, P. T. H.; Santos, A. F.; Yamamoto, C. I.; Tose, L. V.; Barros, E. V.; Gonçalves, G. R.; Freitas, J. C. C.; Vaz, B. G.; Romão, W.; Scheer, A. P. Fractionation of Asphaltene by Adsorption onto Silica and Chemical Characterization by Atmospheric Pressure Photoionization Fourier Transform Ion Cyclotron Resonance Mass Spectrometry, Fourier Transform Infrared Spectroscopy Coupled to Attenuated Total Reflectance, and Proton Nuclear Magnetic Resonance. *Energy Fuels* **2016**, *30* (7), 5439−5448.

(19) Speight, J. G. Petroleum Asphaltenes—Part 2: The Effect of Asphaltene and Resin Constituents on Recovery and Refining Processes. *Oil Gas Sci. Technol.* **2004**, *59* (5), 479−488.

(20) Garcia-Montoto, V.; Verdier, S.; Maroun, Z.; Egeberg, R.; Tiedje, J. L.; Sandersen, S.; Zeuthen, P.; Bouyssiere, B. Understanding the removal of V, Ni and S in crude oil atmospheric residue hydrodemetallization and hydrodesulfurization. *Fuel Process. Technol.* **2020**, *201*, 106341.

(21) Caumette, G.; Lienemann, C. P.; Merdrignac, I.; Bouyssiere, B.; Lobinski, R. Fractionation and speciation of nickel and vanadium in crude oils by size exclusion chromatography-ICP MS and normal phase HPLC-ICP MS. *J. Anal. At. Spectrom.* **2010**, *25* (7), 1123−1129.

(22) Gascon, G.; Negrín, J.; Montoto, V. G.; Acevedo, S.; Lienemann, C.-P.; Bouyssiere, B. Simplification of Heavy Matrices by Liquid−Solid Extraction: Part II—How to Separate the LMW, MMW, and HMW Compounds in Asphaltene Fractions for V, Ni, and S Compounds. *Energy Fuels* **2019**, *33* (9), 8110−8117.

(23) Savoca, M.; Wende, T.; Jiang, L.; Langer, J.; Meijer, G.; Dopfer, O.; Asmis, K. R. Infrared Spectra and Structures of Silver−PAH Cation Complexes. *J. Phys. Chem. Lett.* **2011**, *2* (16), 2052−2056.

(24) Griffith, E. A. H.; Amma, E. L. Metal ion-aromatic complexes. XVIII. Preparation and molecular structure of naphthalenetetrakis-(silver perchlorate) tetrahydrate. *J. Am. Chem. Soc.* **1974**, *96* (3), 743−749.

(25) Heshka, N. E.; Baltazar, M.; Chen, J. Separation and quantification of olefins and diolefins in cracked petroleum fractions using silver-ion high performance liquid chromatography. *Pet. Sci. Technol.* **2019**, *37* (15), 1808−1816.

(26) Eftekhari, M.; Ismail, A. I.; Zare, R. N. Isomeric differentiation of polycyclic aromatic hydrocarbons using silver nitrate reactive desorption electrospray ionization mass spectrometry. *Rapid Commun. Mass Spectrom.* **2012**, *26* (17), 1985−1992.

(27) Roussis, S. G.; Proulx, R. Molecular Weight Distributions of Heavy Aromatic Petroleum Fractions by Ag$^+$ Electrospray Ionization Mass Spectrometry. *Anal. Chem.* **2002**, *74* (6), 1408−1414.

(28) Bennett, B.; Larter, S. R. Quantitative Separation of Aliphatic and Aromatic Hydrocarbons Using Silver Ion−Silica Solid-Phase Extraction. *Anal. Chem.* **2000**, *72* (5), 1039−1044.

(29) Lobodin, V. V.; Robbins, W. K.; Lu, J.; Rodgers, R. P. Separation and Characterization of Reactive and Non-Reactive Sulfur

in Petroleum and Its Fractions. *Energy Fuels* **2015**, *29* (10), 6177−6186.

(30) Nair, S.; Tatarchuk, B. J. Supported silver adsorbents for selective removal of sulfur species from hydrocarbon fuels. *Fuel* **2010**, *89* (11), 3218−3225.

(31) Mennito, A. S.; Qian, K. Characterization of Heavy Petroleum Saturates by Laser Desorption Silver Cationization and Fourier Transform Ion Cyclotron Resonance Mass Spectrometry. *Energy Fuels* **2013**, *27* (12), 7348−7353.

(32) Moulian, R.; Zheng, F.; Salvato Vallverdu, G.; Barrere-Mangote, C.; Shi, Q.; Giusti, P.; Bouyssiere, B. Understanding the Vanadium−Asphaltene Nanoaggregate Link with Silver Triflate Complexation and GPC ICP-MS Analysis. *Energy Fuels* **2020**, *34* (11), 13759−13766.

(33) Giraldo-Dávila, D.; Chacón-Patiño, M. L.; McKenna, A. M.; Blanco-Tirado, C.; Combariza, M. Y. Correlations between Molecular Composition and Adsorption, Aggregation, and Emulsifying Behaviors of PetroPhase 2017 Asphaltenes and Their Thin-Layer Chromatography Fractions. *Energy Fuels* **2018**, *32* (3), 2769−2780.

(34) Acevedo, N.; Moulian, R.; Chacón-Patiño, M. L.; Mejia, A.; Radji, S.; Daridon, J.-L.; Barrère-Mangote, C.; Giusti, P.; Rodgers, R. P.; Piscitelli, V.; Castillo, J.; Carrier, H.; Bouyssiere, B. Understanding Asphaltene Fraction Behavior through Combined Quartz Crystal Resonator Sensor, FT-ICR MS, GPC ICP HR-MS, and AFM Characterization. Part I: Extrography Fractionations. *Energy Fuels* **2020**, *34* (11), 13903−13915.

(35) Chacón-Patiño, M. L.; Rowland, S. M.; Rodgers, R. P. Advances in Asphaltene Petroleomics. Part 2: Selective Separation Method That Reveals Fractions Enriched in Island and Archipelago Structural Motifs by Mass Spectrometry. *Energy Fuels* **2018**, *32* (1), 314−328.

(36) Putman, J. C.; Gutiérrez Sama, S.; Barrère-Mangote, C.; Rodgers, R. P.; Lobinski, R.; Marshall, A. G.; Bouyssière, B.; Giusti, P. Analysis of Petroleum Products by Gel Permeation Chromatography Coupled Online with Inductively Coupled Plasma Mass Spectrometry and Offline with Fourier Transform Ion Cyclotron Resonance Mass Spectrometry. *Energy Fuels* **2018**, *32* (12), 12198−12204.

(37) Chacón-Patiño, M. L.; Rowland, S. M.; Rodgers, R. P. Advances in Asphaltene Petroleomics. Part 1: Asphaltenes Are Composed of Abundant Island and Archipelago Structural Motifs. *Energy Fuels* **2017**, *31* (12), 13509−13518.

(38) Chacón-Patiño, M. L.; Moulian, R.; Barrère-Mangote, C.; Putman, J. C.; Weisbrod, C. R.; Blakney, G. T.; Bouyssiere, B.; Rodgers, R. P.; Giusti, P. Compositional Trends for Total Vanadium Content and Vanadyl Porphyrins in Gel Permeation Chromatography Fractions Reveal Correlations between Asphaltene Aggregation and Ion Production Efficiency in Atmospheric Pressure Photoionization. *Energy Fuels* **2020**, *34* (12), 16158−16172.

(39) Acevedo, N.; Vargas, V.; Piscitelli, V.; Le Beulze, A.; Bouyssiere, B.; Carrier, H.; Castillo, J. $SiO_2$ Biogenic Nanoparticles and Asphaltenes: Interactions and Their Consequences Investigated by QCR and GPC-ICP-HR-MS. *Energy Fuels* **2021**, *35* (8), 6566−6575.

(40) Gutierrez Sama, S.; Desprez, A.; Krier, G.; Lienemann, C.-P.; Barbier, J.; Lobinski, R.; Barrere-Mangote, C.; Giusti, P.; Bouyssiere, B. Study of the Aggregation of Metal Complexes with Asphaltenes Using Gel Permeation Chromatography Inductively Coupled Plasma High-Resolution Mass Spectrometry. *Energy Fuels* **2016**, *30* (9), 6907−6912.